

Asymptotic analysis of spatially inhomogeneous stiff and ultra-stiff cosmologies

A. A. Coley* and W. C. Lim†

Department of Mathematics and Statistics, Dalhousie University

Halifax, Nova Scotia, Canada B3H 3J5

We calculate analytically the past asymptotic decay rates close to an initial singularity in general G_0 spatially inhomogeneous perfect fluid models with an effective equation of state which is stiff or ultra-stiff (i.e., $\gamma \geq 2$). These results are then supported by numerical simulations in a special class of G_2 cosmological models. Our analysis confirms and extends the BKL conjectures and lends support to recent isotropization results in cosmological models of current interest (with $\gamma > 2$).

I. INTRODUCTION

The conjectures of Belinskii, Khalatnikov and Lifshitz (BKL) [1] assert that the structure of space-time singularities in general relativity (GR) have the following properties (for a perfect fluid with $\gamma \leq 2$, where $(\gamma - 1) \equiv p/\rho$ is defined as the ratio of the pressure p to the energy density ρ): 1. Each spatial point evolves towards the singularity as if it were a spatially homogeneous cosmology. 2. Space-times with non-stiff matter, $\gamma < 2$, have the property that asymptotically close to the singularity matter is not dynamically significant and the singularities in generic four dimensional space-times are space-like and oscillatory (mixmaster behavior). 3. In the case of stiff matter, $\gamma = 2$, the matter is not insignificant near the singularity (leading to non-oscillatory behavior) and generically have anisotropic singularities which are space-like and non-oscillatory.

We shall investigate the BKL conjectures in cosmological models with an effective equation of state $\gamma = 2$ and extend them to models with $\gamma > 2$ by calculating the past asymptotic decay rates in general (G_0) spatially inhomogeneous models. These results are then

*Electronic address: aac@mathstat.dal.ca

†Electronic address: wclim@mathstat.dal.ca

supported by a numerical analysis of the behavior of spatially inhomogeneous solutions to Einstein's equations near an initial singularity in a special class of Abelian G_2 spatially inhomogeneous models.

There are a number of cosmological models of current physical interest which have an effective equation of state $\gamma \geq 2$. Although a complete fundamental theory is not presently known the phenomenological consequences can be understood by studying an effective low-energy theory, which leads to the introduction of additional fields (e.g., scalar fields) in the high curvature regime close the Planck time scale. Scalar fields are believed to be abundant and pervasive in all fundamental theories of physics applicable in the early Universe, particularly in dimensionally reduced higher-dimensional theories [2, 3]. In addition, scalar field cosmological models are of great importance in the study of the early Universe, particularly in the investigation of inflation [3, 4] and “quintessence” scalar field models [5] consistent with observations of the present accelerated cosmic expansion [6]. Superstring theory represents the most promising candidate for a unified theory of the fundamental interactions, including gravity [2]. It is widely believed that eleven-dimensional supergravity represents the low-energy limit of M -theory [7]. In the low-energy limit, to lowest-order in both the string coupling and the inverse string tension, all massive modes in the superstring spectrum decouple and only the massless sectors remain, which are determined by the corresponding supergravity actions. A definitive prediction of string theory is the existence of a scalar field, known as the dilaton, interpreted as a modulus field parametrizing the radius of the eleventh dimension. There are two further massless excitations that are common to all five perturbative string theories, namely the metric tensor field (the graviton) and an anti-symmetric form field. When the higher-dimensional metric is compactified, additional form fields and scalar moduli fields are produced. Thus the low-energy effective action of the theory essentially reduces to GR plus massless scalar fields. A massless scalar field (or moduli field etc.) close to the initial singularity has an effective equation of state $\gamma = 2$.

Models in which $\gamma \geq 2$ arise naturally in ekpyrotic [8] and cyclic [9] cosmological models, which have a big crunch/big bang transition with a contraction phase dominated by a scalar field with $\gamma \geq 2$ to the future [10]. In particular, it was shown [11] that if $\gamma > 2$, chaotic mixmaster oscillations due to anisotropy and curvature are suppressed and the contraction is described by a spatially homogeneous and isotropic evolution. This result was subsequently generalized to theories where the scalar field couples to p -forms, and it was also shown that

\mathbb{Z}_2 orbifold compactification also contributes to suppressing chaotic behavior. Indeed, it was concluded that chaos is avoided in contracting heterotic M -theory models if $\gamma > 2$ at the crunch.

There is currently great interest in higher-dimensional gravity theories inspired by string theory in which the matter fields are confined to a 3+1-dimensional “brane-world” embedded in higher dimensions, while the gravitational field can also propagate in the extra bulk dimensions [12]. There has been particular interest in the dynamics of the Universe at early times in Randall-Sundrum-type brane-world cosmological models [13]. A unique feature of brane cosmology is that ρ^2 dominates at early times, leading to an effective equation of state parameter with $\gamma > 2$, which will give rise to completely different behavior to that in GR. The cosmological implications of brane world models have been extensively investigated [14]. In particular, it was found that an isotropic singularity is a past-attractor in all orthogonal Bianchi models [15]. Moreover, the asymptotic dynamical evolution of spatially inhomogeneous brane-world cosmological models close to the initial singularity was studied numerically [16] and it was found that there always exists an initial singularity, characterized by the fact that spatial derivatives are dynamically negligible, which is isotropic for all physical parameter values. The numerical results were supported by a qualitative dynamical analysis and a calculation of the past asymptotic decay rates [16].

Andersson and Rendall [17] proved that a generic inhomogeneous cosmology with a stiff fluid or a scalar field tends to a velocity-dominated solution, which is the Jacobs solution [18, p. 1426], along individual timelines. For a generic inhomogeneous cosmology with $\gamma > 2$, we will show that it tends to a flat isotropic solution¹ along individual timelines. Note that these solutions are self-similar [21]. In this paper we shall show that these results are supported by the calculations of past asymptotic decay rates in general G_0 models (with $\gamma \geq 2$)² and numerical simulations in a class of G_2 models with one tilt degree of freedom.

¹ Namely the Binétruy, Deffayet and Langlois solution [19], which is essentially the flat Friedmann-Lemaître solution [20, Ch. 2] with $\gamma > 2$.

² We assume that a massless scalar field (or a massive scalar field close to the initial singularity) can be modelled by a perfect fluid with a stiff equation of state. This is justified in detail in [17].

II. ASYMPTOTIC DYNAMICS AT EARLY TIMES FOR G_2 COSMOLOGIES

We first consider the dynamics of a class of G_2 spatially inhomogeneous cosmological models with one spatial degree of freedom. The governing system of evolution equations constitute a system of autonomous partial differential equations in two independent variables. We follow the formalism of [22] which utilizes area expansion-normalized scale-invariant dependent variables, and we use the separable area gauge to consider analytically and numerically the asymptotic evolution of the class of G_2 cosmologies with one tilt degree of freedom³ near the cosmological initial singularity. For recent works on these models (with $\gamma < 2$), we refer to [23]; for vacuum G_2 models, we refer to [24] and references therein. The decay rates at early times can be derived by following the analyses in [25] and [16] by exploiting asymptotic silence.⁴ The results for G_2 models with one tilt degree of freedom are given below.

A. Case $\gamma = 2$

For the case $\gamma = 2$, we assume that the following conditions hold uniformly for open intervals of x .

$$C_1 : \lim_{t \rightarrow -\infty} (E_1^1, A, N_\times, N_-, \Sigma_\times, \Sigma_2, v) = \mathbf{0}, \quad \lim_{t \rightarrow -\infty} (\Sigma_+, \Sigma_-) = (\hat{\Sigma}_+(x), \hat{\Sigma}_-(x))$$

$$C_2 : \partial_x(E_1^1, A, N_\times, N_-, \Sigma_\times, \Sigma_2, v, \Sigma_+, \Sigma_-) \text{ are bounded as } t \rightarrow -\infty.$$

$$C_3 : V = \mathcal{O}(f(t)) \text{ implies } \partial_x V = \mathcal{O}(f(t)) \text{ (asymptotic expansions in time can be differentiated with respect to the spatial coordinates).}$$

The decay rates as $t \rightarrow -\infty$ are then given by

$$(E_1^1, A) = e^{2t}[(\hat{E}_1^1, \hat{A}) + \mathcal{O}(f)] , \quad (\Sigma_+, \Sigma_-, \Omega) = (\hat{\Sigma}_+, \hat{\Sigma}_-, \hat{\Omega}) + \mathcal{O}(g) \quad (1)$$

$$\Sigma_2 = e^{k_1 t}[\hat{\Sigma}_2 + \mathcal{O}(g)] , \quad \Sigma_\times = e^{k_2 t}[\hat{\Sigma}_\times + \mathcal{O}(h)] , \quad N_- = e^{k_3 t}[\hat{N}_- + \mathcal{O}(h)] \quad (2)$$

$$N_\times = e^{2t}[-\hat{E}_1^1 \partial_x \hat{\Sigma}_- t + \hat{N}_\times + \mathcal{O}(h)] , \quad v = e^{2t}[-\frac{1}{2} \hat{E}_1^1 \partial_x \ln \hat{\Omega} t + \hat{v} + \mathcal{O}(h)] \quad (3)$$

³ This class is described by the area expansion rate $\beta \equiv H - \frac{1}{2}\sigma_{11}$ [23, eq. (2.103)] and the normalized variables $(E_1^1, A, N_\times, N_-, \Sigma_\times, \Sigma_2, \Sigma_+, \Sigma_-, \Omega, v)$ defined with respect to a time-like congruence that corresponds to the separable area gauge. E_1^1 is the frame coefficient, A, N_\times, N_- are the components of spatial curvatures, $\Sigma_\times, \Sigma_2, \Sigma_+, \Sigma_-$ are the shears, Ω is the normalized density parameter, and v is the tilt of the perfect fluid. See [23, Appendix D] for the governing equations, where we set $\Lambda = 0$ and evolve β instead [23, eq. (2.108)]. We remind the reader that the logarithmic time variable $t \equiv \ln \ell$ is used.

⁴ See [26] for the notion of the silent boundary and its role in past asymptotic dynamics.

where $\hat{\Sigma}_+ := \frac{1}{2}[1 - \hat{\Sigma}_-^2 - \hat{\Omega}]$, and

$$k_1 = -3\hat{\Sigma}_+ + \sqrt{3}\hat{\Sigma}_-, \quad k_2 = -2\sqrt{3}\hat{\Sigma}_-, \quad k_3 = 2(1 + \sqrt{3}\hat{\Sigma}_-), \quad (4)$$

$$f = e^{4t} + e^{2k_1 t}, \quad g = te^{4t} + e^{2k_1 t} + e^{2k_2 t} + e^{2k_3 t}, \quad h = t(e^{4t} + e^{2k_1 t} + e^{2k_2 t} + e^{2k_3 t}). \quad (5)$$

The area expansion rate β and its associated deceleration parameter satisfy

$$\beta = e^{-3(1-\hat{\Sigma}_+)t}[\hat{\beta} + \mathcal{O}(g)], \quad q = 2 + \mathcal{O}(f). \quad (6)$$

The ten hat variables above are functions of x , and satisfy the two constraints

$$0 = \hat{E}_1^1 \partial_x \ln \hat{\beta} + \hat{r}, \quad 0 = \hat{E}_1^1 \partial_x \ln \hat{\Sigma}_2 - \left[\hat{r} + 3\hat{A} - \sqrt{3}\hat{N}_\times \right], \quad (7)$$

where $\hat{r} = -3\hat{A}\hat{\Sigma}_+ - 3\hat{N}_\times\hat{\Sigma}_- + 3\hat{N}_-\hat{\Sigma}_\times - 3\hat{\Omega}$. That leaves eight hat variables, the same number as when we specify the initial conditions for numerical simulations.⁵ To ensure the convergence of N_- , Σ_\times and Σ_2 , the exponents k_1 , k_2 and k_3 must be positive for all x . This implies that the attractor is confined within the region

$$\Sigma_-^H > -\frac{1}{\sqrt{3}}(1 + \Sigma_+^H), \quad \Sigma_-^H < 0, \quad \Sigma_-^H > \sqrt{3}\Sigma_+^H \quad (8)$$

inside the Kasner circle (triangle I in Figure 3a) in the state space of Hubble-normalized variables, where

$$\Sigma_\pm^H = \frac{\Sigma_\pm}{1 - \Sigma_+}. \quad (9)$$

Note that this restriction is gauge-dependent.

The area expansion-normalized Weyl scalar \mathcal{W} is given by

$$\mathcal{W}^2 = \frac{1}{9}(\hat{\Sigma}_+ - \hat{\Sigma}_-^2)^2 + \frac{1}{9}(1 - 3\hat{\Sigma}_+)^2\hat{\Sigma}_-^2 + \mathcal{O}(g + t^2 e^{4t}). \quad (10)$$

Figure 1 shows the hat variables as computed at $t = -50$ and $t = -100$ for a numerical run (e.g., we plot $e^{-2t}E_1^1$, $e^{-2t}(N_\times + tE_1^1\partial_x\Sigma_-)$, etc).⁶ Since the plots at both times coincide,

⁵ Only six of the hat variables are essential, since we can use the remaining temporal gauge freedom to set $\hat{A} = 0$, and parameterize x to set $\hat{E}_1^1 = 1$.

⁶ For numerical simulations, we use **CLAWPACK**. Since it handles exponential growth rather inaccurately, we evolve the following variables instead:

$$\ln E_1^1, \quad A/E_1^1, \quad \Sigma_-, \quad e^{-2t}N_\times, \quad \ln \Sigma_\times, \quad \ln N_-, \quad \ln \Omega, \quad e^{-2t}\text{artanh}(v), \quad \ln \Sigma_2, \quad \ln \beta.$$

Compare with [23, Appendix D]. One should ensure that Σ_\times and N_- are positive during the simulation.

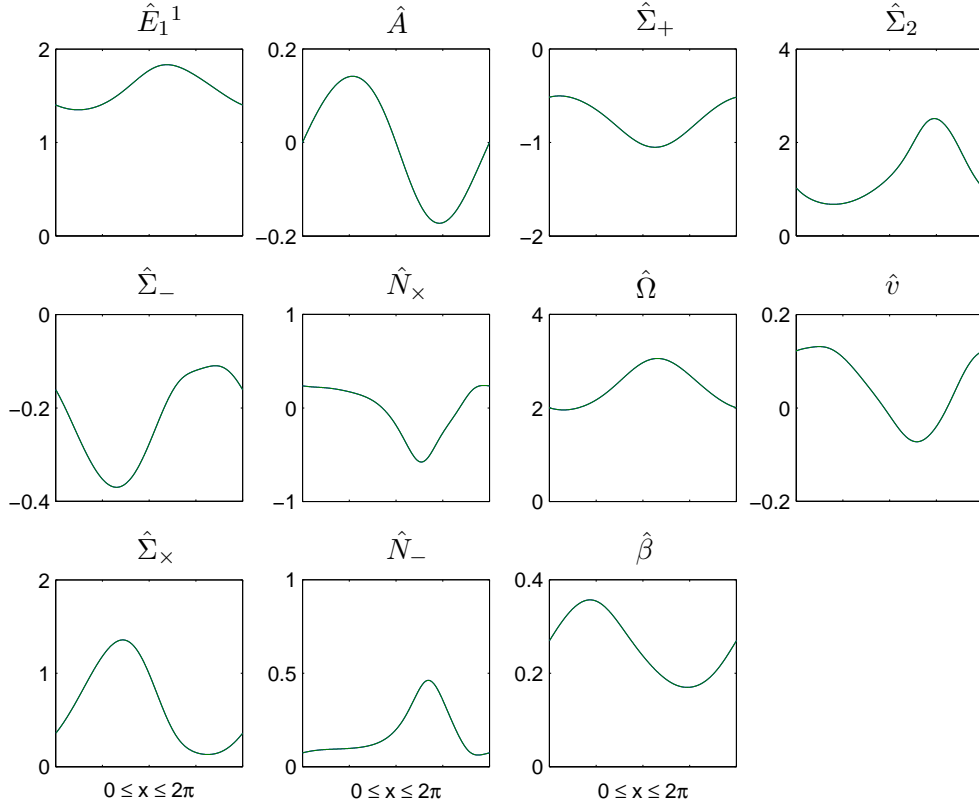


FIG. 1: The hat variables computed at $t = -50$ and $t = -100$ coincide, thus confirming the decay rates.

the decay rates are confirmed. Although the constraints tend to zero, they do not tend to zero fast enough and equation (7) is not satisfied to a sufficient degree of accuracy (this numerical problem can be solved by standard methods). Nonetheless, the numerical results are good enough for confirming the decay rates. The numerical simulations consequently confirm the calculations of the decay rates, provide evidence for the conditions C_1 – C_3 , and hence lend support to the conjectures formulated above.

We use 32768 grid points with periodic boundary condition, and run the simulation from $t = 0$ to $t = -100$. For the initial condition, we set $\gamma = 2$, $\beta_0 = 1$ and

$$\epsilon = 0.1, (E_1^1)_0 = 1, A_0 = 0, (\Sigma_-)_0 = -0.2, (\Sigma_x)_0 = 0.2, (N_-)_0 = 0.2, \Omega_0 = 1, (\Sigma_2)_0 = 0.4$$

in conjunction with [23, eq. (9.1)].

B. Case $\gamma > 2$

For the case $\gamma > 2$, we assume that the following conditions hold uniformly for open intervals of x .

$$C_1 : \lim_{t \rightarrow -\infty} (E_1^1, A, N_\times, N_-, \Sigma_+, \Sigma_-, \Sigma_\times, \Sigma_2, v) = \mathbf{0},$$

$$C_2 : \partial_x(E_1^1, A, N_\times, N_-, \Sigma_\times, \Sigma_2, v, \Sigma_+, \Sigma_-) \text{ are bounded as } t \rightarrow -\infty.$$

$$C_3 : V = \mathcal{O}(f(t)) \text{ implies } \partial_x V = \mathcal{O}(f(t)) \text{ (asymptotic expansions in time can be differentiated with respect to the spatial coordinates).}$$

The decay rates as $t \rightarrow -\infty$ are then given by

$$(E_1^1, A, N_-, N_\times, v) = \eta \left[(\hat{E}_1^1, \hat{A}, \hat{N}_-, \hat{N}_\times, \hat{v}) + \mathcal{O}(\xi) \right] \quad (11)$$

$$(\Sigma_+, \Sigma_-, \Sigma_\times, \Sigma_2, \Omega - 1) = \xi \left[(\hat{\Sigma}_+, \hat{\Sigma}_-, \hat{\Sigma}_\times, \hat{\Sigma}_2, -2\hat{\Sigma}_+) + \mathcal{O}(\xi) \right] \quad (12)$$

where

$$\eta = e^{\frac{1}{2}(3\gamma-2)t}, \quad \xi = e^{\frac{3}{2}(\gamma-2)t}. \quad (13)$$

The area expansion rate β and its associated deceleration parameter satisfy

$$\beta = e^{-\frac{3}{2}\gamma t} [\hat{\beta} + \mathcal{O}(\xi)], \quad q = \frac{1}{2}(3\gamma - 2) + \mathcal{O}(\xi). \quad (14)$$

The ten hat variables above are functions of x , and satisfy the two constraints

$$0 = \hat{E}_1^1 \partial_x \ln \beta - \frac{3}{2}\gamma \hat{v}, \quad 0 = \hat{E}_1^1 \partial_x \ln \hat{\Sigma}_2 - \left(-\frac{3}{2}\gamma \hat{v} + 3\hat{A} - \sqrt{3}\hat{N}_\times\right). \quad (15)$$

That leaves eight hat variables, the same number as when we specify the initial conditions for numerical simulations.

The area expansion-normalized Weyl scalar \mathcal{W} is given by

$$\mathcal{W}^2 = \frac{1}{9}(\hat{\Sigma}_+^2 + \hat{\Sigma}_-^2 + \hat{\Sigma}_\times^2 + \hat{\Sigma}_2^2)\xi^2 + \mathcal{O}(\xi^3). \quad (16)$$

Figure 2 shows the hat variables as computed at $t = -50$ and $t = -100$ for a numerical run (e.g. plot E_1^1/η , etc).⁷ That the plots at both times coincide confirms the decay rates.⁸ Therefore, we have presented numerical evidence for isotropization in these models.

⁷ For the case $\gamma > 2$, we evolve the variables

$$\ln E_1^1, A/E_1^1, \Sigma_-/\xi, \Sigma_\times/\xi, N_-/\eta, N_\times/\eta, (\Omega - 1)/\xi, \text{artanh}(v)/\eta, \ln \Sigma_2, \ln \beta.$$

We use the same initial condition as before, except with $\gamma = 2.1$.

⁸ We again note that numerically the constraints do not tend to zero sufficiently fast.

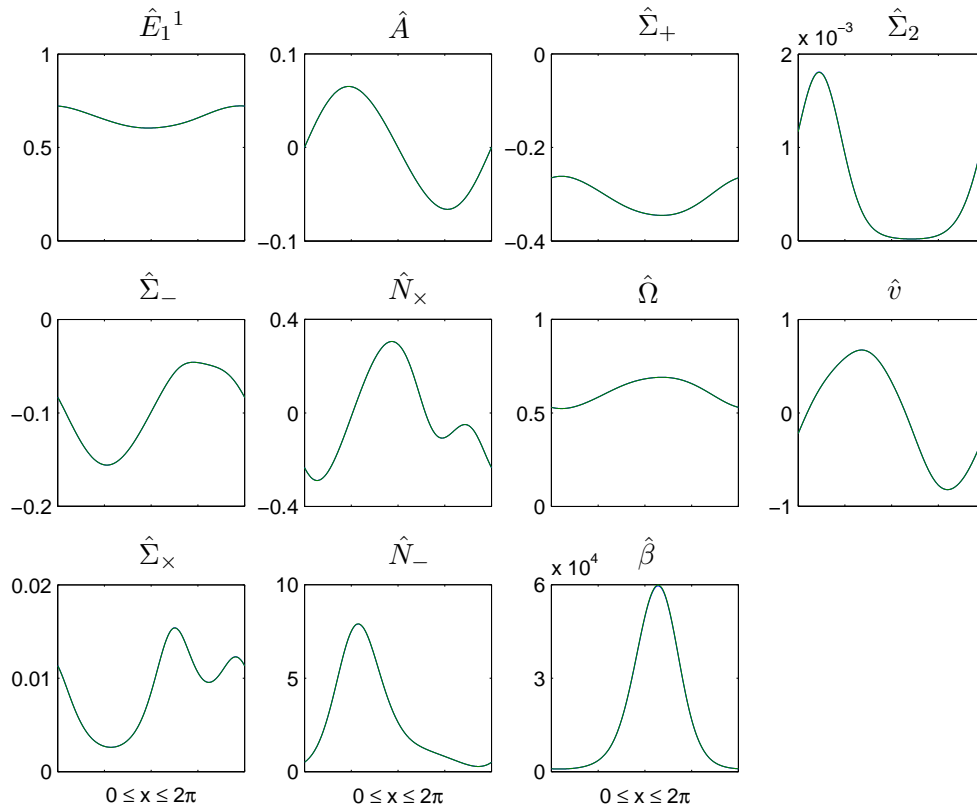


FIG. 2: The hat variables computed at $t = -50$ and $t = -100$ coincide, thus confirming the decay rates.

III. ASYMPTOTIC DYNAMICS AT EARLY TIMES FOR G_0 COSMOLOGIES

It would also be of interest to investigate general inhomogeneous (G_0) models with $\gamma \geq 2$ close to the singularity. We refer to [26] for the equations in the separable volume gauge, using Hubble-normalized variables (where we set $\Lambda = 0$, $R^\alpha = 0$). We give the asymptotic decay rates below. We hope to be able to numerically simulate the G_0 cosmologies in future work.⁹

⁹ Simulation of G_0 cosmologies is expensive and technically difficult. Simulations of vacuum G_0 cosmologies with 50 grid points for each of x^i has been carried out recently [27].

A. Case $\gamma = 2$

For the case $\gamma = 2$, we assume that the following conditions hold uniformly for open sets of x^i .

$$C_1 : \lim_{t \rightarrow -\infty} (E_\alpha^i, A_\alpha, N_{\alpha\beta}, v_\alpha) = \mathbf{0}, \quad \lim_{t \rightarrow -\infty} \Sigma_{\alpha\beta} = \hat{\Sigma}_{\alpha\beta}$$

$$C_2 : \partial_x (E_\alpha^i, A_\alpha, N_{\alpha\beta}, v_\alpha, \Sigma_{\alpha\beta}) \text{ are bounded as } t \rightarrow -\infty.$$

$$C_3 : V = \mathcal{O}(f(t)) \text{ implies } \partial_x V = \mathcal{O}(f(t)) \text{ (asymptotic expansions in time can be differentiated with respect to the spatial coordinates).}$$

Without loss of generality, we perform a spatially-dependent rotation to set $\hat{\Sigma}_{\alpha\beta} = 0$ for $\alpha \neq \beta$. The decay rates as $t \rightarrow -\infty$ are then given by (no summation over repeated indices below)

$$E_\alpha^i = e^{(2-\hat{\Sigma}_{\alpha\alpha})t} [\hat{E}_\alpha^i + \mathcal{O}(F)], \quad r_\alpha = e^{(2-\hat{\Sigma}_{\alpha\alpha})t} [\hat{r}_\alpha + \mathcal{O}(tF)] \quad (17)$$

$$A_\alpha = e^{(2-\hat{\Sigma}_{\alpha\alpha})t} [\frac{1}{2} \hat{E}_\alpha^i \partial_i \hat{\Sigma}_{\alpha\alpha} t + \hat{A}_\alpha + \mathcal{O}(tF)] \quad (18)$$

$$N_{\alpha\alpha} = e^{(2+2\hat{\Sigma}_{\alpha\alpha})t} [\hat{N}_{\alpha\alpha} + \mathcal{O}(tF)] \quad (19)$$

$$N^{\alpha\beta} = e^{(2-\hat{\Sigma}_{\mu\mu})t} [-\hat{E}_\gamma^i \partial_i \epsilon^{\gamma\delta(\alpha\hat{\Sigma}^\beta)}_\delta t + \hat{N}^{\alpha\beta} + \mathcal{O}(tF)], \quad \mu \neq \alpha \neq \beta \quad (20)$$

$$\Omega = \hat{\Omega} + \mathcal{O}(F), \quad v_\alpha = e^{(2-\hat{\Sigma}_{\alpha\alpha})t} [-\frac{1}{2} (\hat{E}_\alpha^i \partial_i \ln \hat{\Omega} - 2\hat{r}_\alpha) t + \hat{v}^\alpha + \mathcal{O}(tF)] \quad (21)$$

$$\Sigma_{\alpha\alpha} = \hat{\Sigma}_{\alpha\alpha} + \mathcal{O}(F), \quad \Sigma_{\alpha\beta} = \mathcal{O}(F), \quad \alpha \neq \beta \quad (22)$$

where

$$F = t^2 e^{2(2-s_+)t} + e^{2(2+2s_-)t}, \quad s_+(x^i) = \max_{\alpha=1,2,3} \hat{\Sigma}_{\alpha\alpha}, \quad s_-(x^i) = \min_{\alpha=1,2,3} \hat{\Sigma}_{\alpha\alpha}.$$

The Hubble scalar and the deceleration parameter satisfy

$$H = e^{-3t} [\hat{H} + \mathcal{O}(F)], \quad q = 2 + \mathcal{O}(F). \quad (23)$$

The twenty eight hat variables above¹⁰ are functions of x^i , and satisfy the following sixteen constraints

$$\hat{r}_\alpha = -\hat{E}_\alpha^i \partial_i \ln \hat{H}, \quad 0 = \hat{E}_\alpha^i \partial_i \hat{\Sigma}_{\alpha\alpha} + (2 - \hat{\Sigma}_{\alpha\alpha}) \hat{r}_\alpha - 3\hat{A}_\alpha \hat{\Sigma}_{\alpha\alpha} - \epsilon_\alpha^{\beta\gamma} \hat{N}_{\beta\delta} \hat{\Sigma}_\gamma^\delta + 6\hat{\Omega} \hat{v}_\alpha, \quad (24)$$

$$\hat{\Omega} = 1 - \frac{1}{6} \left(\hat{\Sigma}_{11}^2 + \hat{\Sigma}_{22}^2 + \hat{\Sigma}_{33}^2 \right), \quad 0 = 2(\hat{E}_{[\alpha}^j \partial_j - \hat{r}_{[\alpha} - \hat{A}_{[\alpha}) \hat{E}_{\beta]}^i - \epsilon_{\alpha\beta\delta} \hat{N}^{\delta\gamma} \hat{E}_\gamma^i. \quad (25)$$

¹⁰ Note that $\hat{\Sigma}_{11} + \hat{\Sigma}_{22} + \hat{\Sigma}_{33} = 0$, and we can write $\hat{\Sigma}_{\alpha\alpha} = \text{diag}(-2\hat{\Sigma}_+, \hat{\Sigma}_+ + \sqrt{3}\hat{\Sigma}_-, \hat{\Sigma}_+ - \sqrt{3}\hat{\Sigma}_-)$.

That leaves twelve hat variables, of which eight are essential, since we can use the remaining temporal gauge freedom to set $\hat{H} = \text{const}$ and make a change of coordinates to set three of the \hat{E}_α^i 's.

Note that $\hat{\Sigma}_{\alpha\alpha}$ satisfy $|\hat{\Sigma}_{\alpha\alpha}| < 2$ by definition. The exponents of $N_{\alpha\alpha}$ must be positive, however, thus requiring that $\hat{\Sigma}_{\alpha\alpha} > -1$; i.e., the Jacobs solutions are restricted within the triangle

$$\Sigma_+ < \frac{1}{2}, \quad -\frac{1}{\sqrt{3}}(1 + \Sigma_+) < \Sigma_- < \frac{1}{\sqrt{3}}(1 + \Sigma_+). \quad (26)$$

See triangle I in Figure 3b.

The Hubble-normalized Weyl scalar \mathcal{W} is given by

$$\mathcal{W}^2 = \frac{1}{9}(\hat{\Sigma}_+ + \hat{\Sigma}_+^2 - \hat{\Sigma}_-^2)^2 + \frac{1}{9}(1 - 2\hat{\Sigma}_+)^2\hat{\Sigma}_-^2 + \mathcal{O}(tF). \quad (27)$$

The work of Andersson and Rendall [17] is more rigorous, but also assumes more (e.g., analyticity). Our results complement their analysis by providing more details on the spatial curvature variables and on the big O terms, and is easier to apply and interpret. We have also discussed the restrictions on the Jacobs disk.

B. Case $\gamma > 2$

For the case $\gamma = 2$, we assume that the following conditions hold uniformly for open sets of x^i .

$$C_1 : \lim_{t \rightarrow -\infty} (E_\alpha^i, A_\alpha, N_{\alpha\beta}, v_\alpha, \Sigma_{\alpha\beta}) = \mathbf{0},$$

$$C_2 : \partial_x(E_\alpha^i, A_\alpha, N_{\alpha\beta}, v_\alpha, \Sigma_{\alpha\beta}) \text{ are bounded as } t \rightarrow -\infty.$$

$$C_3 : V = \mathcal{O}(f(t)) \text{ implies } \partial_x V = \mathcal{O}(f(t)) \text{ (asymptotic expansions in time can be differentiated with respect to the spatial coordinates).}$$

The decay rates as $t \rightarrow -\infty$ are then given by

$$(E_\alpha^i, r_\alpha, A_\alpha, N_{\alpha\beta}, v_\alpha) = \eta \left[(\hat{E}_\alpha^i, \hat{r}_\alpha, \hat{A}_\alpha, \hat{N}_{\alpha\beta}, \hat{v}_\alpha) + \mathcal{O}(\xi) \right] \quad (28)$$

$$\Sigma_{\alpha\beta} = \xi [\hat{\Sigma}_{\alpha\beta} + \mathcal{O}(\xi^2)], \quad \Omega = 1 - \frac{1}{6}\hat{\Sigma}_{\alpha\beta}\hat{\Sigma}^{\alpha\beta}\xi^2 + \mathcal{O}(\xi^4 + \eta^2) \quad (29)$$

where η and ξ are given in (13). The Hubble scalar and the deceleration parameter satisfy

$$H = e^{-\frac{3}{2}\gamma t} [\hat{H} + \mathcal{O}(\xi^2)], \quad q = \frac{1}{2}(3\gamma - 2) + \mathcal{O}(\xi^2). \quad (30)$$

The hat variables above are functions of x^i , and satisfy the following constraints

$$\hat{r}_\alpha = -\hat{E}_\alpha{}^i \partial_i \ln \hat{H}, \quad 0 = 2\hat{r}_\alpha + 3\gamma\hat{v}_\alpha, \quad 0 = 2(\hat{E}_{[\alpha}{}^j \partial_j - \hat{r}_{[\alpha} - \hat{A}_{[\alpha}) \hat{E}_{\beta]}{}^i - \epsilon_{\alpha\beta\delta} \hat{N}^{\delta\gamma} \hat{E}_\gamma{}^i. \quad (31)$$

The Hubble-normalized Weyl scalar \mathcal{W} is given by

$$\mathcal{W}^2 = \frac{1}{9} \cdot \frac{1}{6} \hat{\Sigma}_{\alpha\beta} \hat{\Sigma}^{\alpha\beta} \xi^2 + \mathcal{O}(\xi^3). \quad (32)$$

We comment that the results for G_2 and G_0 cases differ slightly, due to the difference in both the temporal and spatial gauges employed.

IV. DISCUSSION

We have shown analytically (and confirmed numerically for the G_2 models) that for the case $\gamma = 2$, a subset of the Jacobs solutions (triangles I in Figure 3) are locally stable into the past, and for the case $\gamma > 2$ the flat Friedmann-Lemaître solution is locally stable into the past. These results confirm and extend the BKL conjectures, and complement the work of Andersson and Rendall [17]. They are also of current physical interest; for example, they lend support to previous isotropization results [11, 28].

In applications to specific physical theories, it may be necessary to investigate the robustness of these results in the presence of certain additional fields. For example, string and M -theories were discussed in order to motivate the existence of a scalar field (dilaton) in the early universe. However, in these theories there are also p -form fields present, which can lead to oscillatory behavior close to the cosmological singularity [29].

We comment that the conditions C_1 – C_3 in Section II A can sometimes be violated in a neighbourhood of isolated timelines $x = \text{const}$, where formation of spiky spatial structures are observed numerically. In a preliminary numerical investigation for the stiff G_2 case, these structures appear to be similar to the spikes in vacuum models [24] and in models with $\gamma < 2$ [23]. We conjecture that the limits for Σ_+ and Σ_- along spike timelines reside in the following two triangles: (i) for true spikes, the limits reside in the triangle

$$-\frac{2}{\sqrt{3}}(1 + \Sigma_+^H) < \Sigma_-^H < -\frac{1}{\sqrt{3}}(1 + \Sigma_+^H), \quad \Sigma_-^H > \sqrt{3}\Sigma_+^H, \quad (33)$$

(ii) for false spikes, the limits reside in the triangle

$$\Sigma_-^H < \frac{1}{\sqrt{3}}(1 + \Sigma_+^H), \quad \Sigma_-^H > 0, \quad \Sigma_-^H < -\sqrt{3}\Sigma_+^H \quad (34)$$

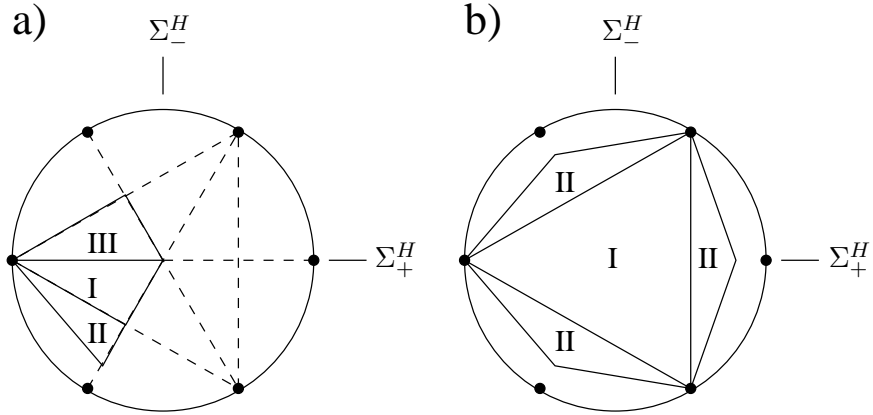


FIG. 3: a) For the stiff G_2 case, the Jacobs solutions that act as the past attractor are confined within triangle I. The limits along the conjectured true and fake spike timelines are confined within triangles II and III respectively. b) For the stiff G_0 case, the Jacobs solutions that act as the past attractor are confined within triangle I. The limits along the conjectured true spike timelines are confined within triangles II.

(see triangles II and III in Figure 3a respectively). We conjecture that true spikes are physically real, and are reflected by a discontinuous limit for the Weyl scalar. On the other hand, false spikes are artifacts of the rotating frame, and are reflected by a continuous limit for the Weyl scalar. It is of interest to study these spikes in more detail.

Similarly, for the stiff G_0 case we conjecture that spikes occur when the limits of $\Sigma_{\alpha\alpha}$ are discontinuous. When this occurs, the limits are confined to the three triangles

$$0 < 4 + 2\Sigma_{\alpha\alpha} - \Sigma_{\beta\beta} , \quad \hat{\Sigma}_{\alpha\alpha} < -1 , \quad (35)$$

for all $\alpha \neq \beta$ (see triangles II in Figure 3b; also compare with [18, Figure 3]).

Acknowledgments

This work was supported by NSERC of Canada. We would like to thank Henk van Elst, Claes Uggla and Alan Rendall for their helpful comments.

-
- [1] E. M. Lifshitz and I. M. Khalatnikov, *Adv. Phys.* **12**, 185 (1963); V. A. Belinskii, I. M. Khalatnikov and E. M. Lifshitz, *Adv. Phys.* **19**, 525 (1970); *Sov. Phys. JETP* **36**, 591 (1973).
 - [2] M. B. Green, J. H. Schwarz, and E. Witten, *Superstring Theory* (Cambridge University Press, 1987); J. Polchinski, *String Theory* (Cambridge University Press, Cambridge, 1998).
 - [3] K. A. Olive, *Phys. Rep.* **190**, 307 (1990).
 - [4] A. H. Guth, *Phys. Rev.* **D23**, 347 (1981); A. Linde, *Inflation and quantum cosmology*, in *300 Years of Gravitation*, ed. S. W. Hawking and W. Israel, pp 604–630 (Cambridge University Press, Cambridge, 1987).
 - [5] R. R. Caldwell, R. Dave and P. J. Steinhardt, *Phys. Rev. Lett.* **80**, 1582 (1998).
 - [6] S. Perlmutter et al., *Astrophys. J.* **517**, 565 (1999); A. G. Riess et al., *Astron. J.* **116**, 1009 (1998).
 - [7] E. Witten, *Nucl. Phys.* **B443**, 85 (1995).
 - [8] J. Khoury, B. A. Ovrut, P. J. Steinhardt and N. Turok, *Phys. Rev. D* **64**, 123522 (2001).
 - [9] P. J. Steinhardt and N. Turok, *Science* **296**, 1436 (2002); *Phys. Rev. D* **65**, 126003 (2002).
 - [10] J. Khoury, P. J. Steinhardt and N. Turok, *Phys. Rev. Lett.* **92** 031302 (2004).
 - [11] J. K. Erickson, D. H. Wesley, P. J. Steinhardt and N. Turok, *Phys. Rev. D* **69** 063514 (2004).
 - [12] V. Rubakov and M. Shaposhnikov, *Phys. Lett. B***159**, 22 (1985); J. Polchinski, *Phys. Rev. Lett.* **75**, 4724 (1995).
 - [13] L. Randall and R. Sundrum, *Phys. Rev. Lett.* **83**, 3370 (1999); *ibid* **83**, 4690 (1999).
 - [14] R. Maartens, *Phys. Rev. D***62**, 084023 (2000); R. Maartens, *Living Reviews in Relativity* **7**, 1 (2004)
 - [15] A. A. Coley, *Phys. Rev. D* **66**, 023512 (2002); A. Coley, *Class. Quant. Grav.* **19**, L45 (2002).
 - [16] A. A. Coley, Y. He and W. C. Lim, *Class. Quant. Grav.* **21**, 1311 (2004)
 - [17] L. Andersson and A. D. Rendall, *Commun. Math. Phys.* **218**, 479 (2001)
 - [18] J. Wainwright and L. Hsu, *Class. Quant. Grav.* **6**, 1409 (1989)

- [19] P. Binétruy, C. Deffayet, and D. Langlois, Nucl. Phys. B**565**, 269 (2000)
- [20] J. Wainwright and G. F. R. Ellis (editors), *Dynamical Systems in Cosmology*, Cambridge University Press (1997).
- [21] B. J. Carr and A. A. Coley, Class. Q. Grav. **16**, R31 (1999).
- [22] H. van Elst, C. Uggla and J. Wainwright, Class. Quantum Grav. **19**, 51 (2002).
- [23] W. C. Lim, PhD thesis, University of Waterloo (2004) [gr-qc/0410126].
- [24] L. Andersson, H. van Elst, W. C. Lim and C. Uggla, Phys. Rev. Lett. **94**, 051101 (2005).
- [25] W. C. Lim, H. van Elst, C. Uggla and J. Wainwright, Phys. Rev. D **69**, 103507 (2004).
- [26] C. Uggla, H. van Elst, J. Wainwright and G. F. R. Ellis, Phys. Rev. D **68**, 103502 (2003).
- [27] D. Garfinkle, Phys. Rev. Lett. **93**, 161101 (2004).
- [28] P. K. S. Dunsby, N. Goheer, M. Bruni and A. Coley, Phys. Rev. D **69**, 101303 (2004).
- [29] T. Damour and M. Henneaux, Phys. Rev. Lett. **85**, 920 (2000); T. Damour, M. Henneaux, A. D. Rendall and M. Weaver, Ann. H. Poincaré **3**, 1049 (2002).